*Desalination and Water Treatment*
www.deswater.com
doi: 10.5004/dwt.2023.30149

315 (2023) 373–386
December

# Synthesis of silver nanoparticles using *Pongamia pinnata* leaf extract for efficient removal of acid Brilliant Red 3BN dye under solar irradiation

R. Sukanya Devi*, Bhaarathi Dhurai

*Department of Textile Technology, Kumaraguru College of Technology, Coimbatore, India, Tel.: +91 422 2661160; emails: sukanyadevi.r.txt@kct.ac.in (R. Sukanya Devi), bhaarathidhurai.txt@kct.ac.in (B. Dhurai)*

Received 9 September 2023; Accepted 20 November 2023

**ABSTRACT**

The degradation of dye in effluent from textile industries is a vital area of research for mitigating the effects of the dyestuff on the ecosystem. In this study, silver nanoparticles were synthesized using a green approach using *Pongamia pinnata* leaf extract as a natural reducing and capping agent. The leaf extract and synthesized silver nanoparticles (AgNPs) were characterized for identifying the active functional groups and UV absorbance. Further, the surface morphology, particle-size distribution, and elemental analysis of the silver nanoparticle were characterized. The photocatalytic studies of the synthesized AgNPs were done for acid dye – acid Brilliant Red 3BN under solar irradiation. The process variables like the dye concentration, contact time, catalyst concentration, and pH were analyzed by one factor at a time approach. The formation of silver nanoparticles from silver nitrate by *P. pinnata* leaf extract was evident at 432 nm. The average particle size was found to be 50 nm and the shape of the silver nanoparticle was spherical. The elemental analysis confirms the presence of silver nanoparticles. The optimum factors are 5 ppm of dye concentration, and 10 mg/L catalyst concentration with a reaction time of 2 h at pH 4 for achieving photocatalytic degradation of 74% of acid Brilliant Red 3BN dye. The kinetic studies reveal that the reaction showed a good fit for the first-order kinetics with a rate constant of 0.00577 $min^{-1}$ with $R^2$ value of 0.97629. This study confirms the green synthesis of silver nanoparticles and its effective degradation of acid Brilliant Red 3BN dye.

*Keywords* : *Pongamia pinnata*; Silver nanoparticle; Acid dyes; Photocatalysis; Solar irradiation; Green synthesis

## 1. Introduction

Water is an essential resource for all living beings. Consumption of fresh water for human needs has been increasing by 1% per year amounting to a six-fold increase in the past 100 years [1]. The quality of available freshwater is affected by industrial activities, agricultural production, and improper urban usage that lead to pollution in water bodies which results in a threat to living beings [2]. There is a rapid increase in the release of various contaminants into water bodies by industries such as textiles, cosmetics, leather, plastics, etc [3]. In particular, the textile and fashion industry contributes, to 2% of the world's total gross domestic product. It is observed from the past two decades that the consumption of textiles per person has increased from 7 to 13 kg, thereby producing 100 million tons of textiles [4]. Chemical processing is an essential step in the manufacturing of textiles. Apart from chemicals used in the process, synthetic dyes are utilized for imparting color to the textiles. Synthetic dyes contain different types of chromophores, among which the azo group (–N=N–) tops the list. The removal of dyes from wastewater is difficult as most of the dyes are non-biodegradable. Destruction of the azo bond in the wastewater is essential for rendering the water harmless for further use [5].

* Corresponding author.

Several treatment methods such as adsorption using low-cost adsorbents, chemical methods like the Fenton process, ozonation, electrocoagulation, and membrane technologies like ultrafiltration, reverse osmosis, etc., are adopted to treat the wastewater discharged from the textile wet processing industry [6]. Although various technologies are established for the treatment of wastewater, the implementation of the methods in the industry on a large scale is a challenge for obtaining maximum efficiency at low operational cost. To meet the demands of the current wastewater treatment challenges, the development of new effective techniques is required [7]. Out of the new emerging technologies, nano-hybrid technology is a promising technique for treating wastewater, and the nanomaterials are used as catalysts in the treatment [8,9]. Photocatalysis is a promising treatment method that uses light sources (usually in UV and visible range bands) and catalysts that liberate reactive oxygen species in the presence of light. The difference in oxidation potential between the reactive oxygen species and the dye leads to a gain or loss of electrons, thereby degrading the dyes. Metal or metal oxide catalysts are generally studied for their photocatalytic properties.

Nanoparticles are an emerging field because of their enhanced catalytic activity. Silver nanoparticles (AgNPs) have gained importance due to their wide application in photonics, photocatalysis, antibacterial applications, etc. [10]. Green synthesis is a potential alternative to chemical synthesis. Compounds from the natural origin are extensively studied for reducing and/or stabilizing the conversion of silver to silver nanoparticles [11,12] Compounds used for the synthesis of AgNPs are extracted from microbes like fungi, bacteria, yeast and algae or from any part of plant extracts that are environment friendly and safe [13]. Synthesis of AgNPs was explored using a variety of plants like the *Acorus calamus*, leaves of *Azadirachta indica*, *Alternanthera dentata*, *Ocimum sanctum*, *Aloe barbadensis* Mill., *Brassica rapa*, *Syzygium cumini*, *Coccinia indica*, and *Morus* by previous researchers [14–18]. A wide range of phytochemicals are available in plant extracts that have the potential to reduce and stabilize the metal salt into metallic nanoparticles [19–23]. The conditions maintained during green synthesis are responsible for the size and shape of synthesized AgNPs. These factors greatly influence the dye degradation activity of the photocatalyst [24,25].

*Pongamia pinnata*, a tree species in the pea family, is a native of the eastern and tropical Asia, Australia and the Pacific islands. It is commonly called as Indian beech and Pongame oil tree. The trees are found in surplus in India and are known for its high oxygen transfer to the environment. The leaves of *P. pinnata* are rich in polyphenols and flavonoids that have hydroxyl and ketonic groups which easily bind with the metals and reduce them to nanoparticles [26]. Also, these groups provide stability against agglomeration. The plant extract furnishes protein and enzymes to the silver nitrate solution in which silver ions combine with the enzymes to form an enzyme-substrate complex to release silver nanoparticles, while the proteins act as a capping agent to prevent the agglomeration of the nanoparticles.

The present study uses a green approach of synthesizing silver nanoparticles using *P. pinnata* leaf which is an abundant resource. The leaves are collected and incinerated or left for natural biodegradation. The study reveals that the leaf extract can act as a reducing and capping agent in the synthesis of AgNPs. The synthesized AgNPs were characterized for their shape, size, elemental analysis, functional groups, absorbance value and crystal size. Most of the photocatalytic studies using AgNPs were carried out for the degradation of cationic dyes. But in this study, Colomill Brilliant Red 3BN, an anionic dye that is widely used by the silk and nylon dyeing industry is considered for the study. The photocatalytic degradation of the dyes was carried out under solar irradiation, by varying the dye concentration, catalyst concentration, time, and pH. The novelty of this study is the usage of abundantly available *P. pinnata* leaf and widely used acid dye for degradation studies.

## 2. Materials and method

### 2.1. Materials

Silver nitrate ($AgNO_3$) of (99.99%) purity was purchased from Sigma-Aldrich, India. *P. pinnata* leaves were collected from Coimbatore, Tamil Nadu, India. Colomill Brilliant Red 3BN (C.I. Acid Red 131) synthetic dye was purchased from Colourtex, Surat. The selected dye was an azo dyestuff classified under acid dye bearing the chemical name disodium 5-(benzoylamino)-4-hydroxy-3-[[2-(2-methylphenoxy)phenyl]azo]naphthalene-2,7-disulphonate with the chemical formula of $C_{30}H_{23}N_3O_9S_2{\cdot}2Na$. The dye molecules have a net negative charge. Ethanol ($C_2H_5OH$) was used for sterilization. Deionized water was used for preparing all the solutions. The chemicals were used without any purification in the experiments.

### 2.2. Extraction of P. pinnata leaf extract

*P. pinnata* leaves were collected locally and washed with distilled water. The leaves were shredded and sterilized with ethanol. 50 g of leaves were taken in 500 mL of double distilled water in an Erlenmeyer flask and boiled at 90°C for 2 h and cooled to room temperature. The colour of the extract was pale yellow and the extract was filtered using a Whatman filter paper No.1 and stored at room temperature for further use.

### 2.3. Synthesis of silver nanoparticles

10 mL of aqueous solution of 0.1 M silver nitrate was prepared with distilled water. This aqueous silver nitrate solution was added to 10 mL of *Pongamia pinnata* leaf extract (PPLE) dropwise with a constant stirring at 350 rpm at room temperature. Due to the addition of the polyphenol and flavonoid rich leaf extract, the silver ions reduced to zero valent silver nanoparticles. The conversion was evidently observed by the change in colour of the solution from pale yellow to dark brown. The reaction continued for 1 h until a stable dark brown solution was obtained. Further, the obtained silver nanoparticles were centrifuged at 13,000 rpm for 5 min at room temperature. After decanting the supernatant, the silver nanoparticles precipitate was washed in deionized water several times. Thus, the obtained silver nanoparticles were suspended in deionized water for characterization and experimentation.

### 2.4. Preparation of synthetic dye effluent

The dye effluent used in this study was simulated by adding 1 g of Colomill Brilliant Red 3BN to 1 L of deionized water and homogenized at 60°C to form the stock solution. Different concentrations of dye effluent were prepared from the stock solution. The maximum absorbance wavelength of this synthetic dye effluent, to measure the concentration was tested using UV-Visible spectrophotometer.

### 2.5. Characterization of silver nanoparticle

The morphological analysis of AgNPs was done using a field emission scanning electron microscope (FE-SEM) of Carl Zeiss (USA), Sigma model with Gemini column. Elemental analysis was done using the Nano Xflash Detector from Bruker, Germany. The particle arrangement of AgNPs in the crystal lattice was studied using X-ray diffraction (XRD) patterns obtained from the X'Pert$^3$ Powder X-ray Diffractometer from Malvern Panalytical (USA). The functional groups present in the plant extract were studied using a Fourier-transform infrared (FTIR) spectrophotometer from Shimadzu, Japan. The absorbance value of the AgNPs was estimated using a double-beam UV-Visible spectrophotometer, Thermo Scientific (Thermo Fisher, USA).

### 2.6. Photocatalytic studies

The dye removal efficiency by photocatalytic reactions was optimized using the OFAT (one-factor-at-a-time) approach. The factors considered were the initial dye concentration, photocatalyst concentration, pH, and time. In OFAT, one factor was varied while the other factors remained unchanged. The synthetic dye with silver nanoparticles was exposed to solar irradiation. The strength of the solar irradiation when monitored by a Luxmeter (Lutron Instruments LX-101A Light Meter, was observed as 70,000 to 90,000 lux during the mid-day. It is approximately 530 to 710 Watts/m$^2$. The treated samples were centrifuged at 10,000 rpm for 10 min to remove AgNPs. The absorption of the samples was measured in a wavelength range of 200–800 nm.

The concentration of the dye was derived from the absorbance values based on Beer–Lamberts law which implies that the quantity of light absorbed by a dye dissolved in water is directly proportional to the concentration of the dye and the path length of the light through the solution. It is mathematically represented in Eq. (1):

$$A = \varepsilon bc \tag{1}$$

where ε is the molar absorptivity, $b$ is the path length of light through the solution, and $c$ is the concentration of the dye.

Similarly, the dye degradation % was calculated using Eq. (2):

$$\text{Dye degradation}(\%) = \left(\frac{C_i - C_f}{C_i}\right) \times 100 \tag{2}$$

where $C_i$ is the initial concentration of the dye solution, $C_f$ is the final concentration of the dye solution.

The mathematical modeling for isotherm and kinetics was analyzed to calculate the maximum degradation capacity. The goodness of the fit was evaluated by $R^2$ value.

## 3. Results and discussion

### 3.1. Characterization of P. pinnata leaf extract

The PPLE was pale yellow in colour. The addition of the leaf extract to the silver nitrate solution changed the colourless liquid to brown colour as shown in Fig. 1. The colourless silver nitrate solution is shown in 1a, the *P. pinnata* leaf extract is shown in Fig. 1b and the reduced brown colour silver nanoparticle is in Fig. 1c. This change in colour due to the excitation of valence electrons in the silver nanoparticle caused surface plasmon resonance and was the indication of the reduction of the silver $Ag^+$ to AgNPs [27]. This reduction of silver nitrate to AgNPs was evident from the UV absorbance curve of PPLE and AgNPs synthesized, where a peak was noted at 432 nm due to the surface plasmon resonance as indicated in Fig. 2. It is suggestive that the polyphenols present in anthocyanin, a flavonoid pigment in *P. pinnata* leaf is responsible for the conversion of $Ag^+$ to AgNPs as it acts as a reducing agent for metallic ions and stabilising the nanoparticles [28,29].

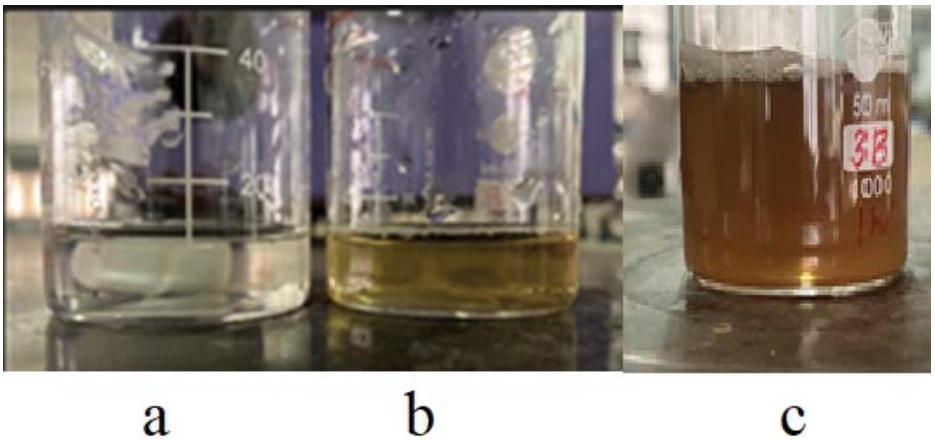


Fig. 1. (a) Silver nitrate solution, (b) *Pongamia pinnata* leaf extract, and (c) silver nanoparticle.

### 3.2. Characterization of silver nanoparticle

#### 3.2.1. Scanning electron microscope and particle size analysis

The FE-SEM micrographs of the AgNPs at 200 nm scale are shown in Fig. 3a. The micrographs show that the AgNPs were almost spherical. No agglomeration of particles was observed. The individual particles could be distinguished thereby confirming that PPLE acts both as a reducing and capping agent. On analysis of particle-size distribution using Image J software, as shown in Fig. 3b, the particles ranged in size from 30 to 100 nm, with the maximum number of particles having the size of 50 nm.

#### 3.2.2. Elemental analysis

In order to confirm the presence of AgNPs, elemental analysis measurement was done. The spectrum in Fig. 4 confirms the presence of AgNPs at 3.0 keV. Similar works [26–28,30] confirmed that the peak of optical absorption occurring around 3 keV was due to the absorption of metallic AgNPs as a result of surface plasmon resonance. The spectrum at 0.2 and 0.6 confirmed carbon and oxygen (O) respectively and this may be due to the presence of organic residues of PPLE.

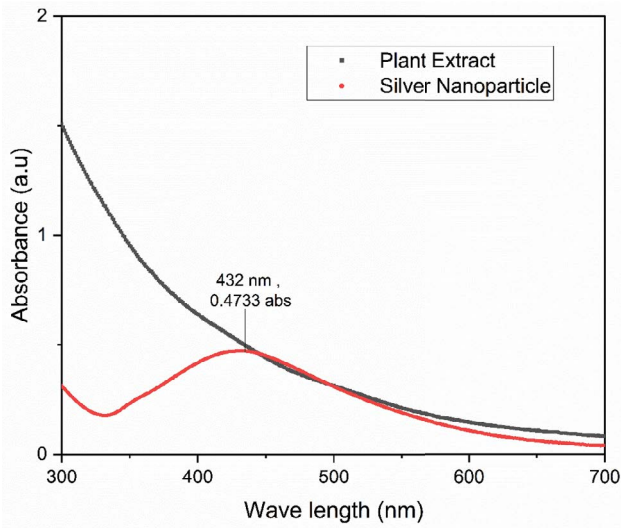


Fig. 2. UV-Visible absorbance curve of PPLE and synthesized AgNP.

#### 3.2.3. FTIR spectrum

The FTIR spectrum was analysed to ascertain the functional groups present in the PPLE and AgNPs. Fig. 5 represents the spectrum showing the functional groups of the phytochemicals present in PPLE were responsible for the reduction and stability of $Ag^+$ to AgNPs. The *P. pinnata* leaf consists of the pongaflavanol, galactoside, pongamol, tunicatachalcone and glybanchalcone [31]. The spectrum showed that silver ions bound with hydroxyl groups and this was visible in a broad band between 3,500 and 3,000 $cm^{-1}$. Peak observed around 1,650 $cm^{-1}$ corresponded to N–H bending of primary amines. C–O functional groups of tannins bound on the surface of the AgNPs. The intensity of the peak between 1,200 and 1,000 $cm^{-1}$ corresponded to the C–O groups of polyphenols such as flavonoids, was reduced in the AgNPs spectrum since the polyphenols were responsible for the reduction of $Ag^+$ to AgNPs. [32,33].

A tentative mechanism of reduction and capping of silver nanoparticles can be found in Fig. 6. The flavonoids which have comparatively less bond disassociation energy than the phenolic compounds, containing two hydroxyl groups –OH facilitates the replacement of $2H^+$ with $2Ag^+$ and further reduce to zerovalent silver and agglomeration is prevented by capping of the alkaloids, saponins, and tannins present in the natural extract on the silver nanoparticles [34,35].

#### 3.2.4. XRD pattern

Fig. 7 shows the XRD pattern of the PPLE synthesized AgNPs, that displayed intense peaks at 2q values of 38.25°, 44.37°, 64.52°, 77.57° and 85.93° correspondingly representing the miller indices (*hkl*) of (111), (200), (220), (311), (222)

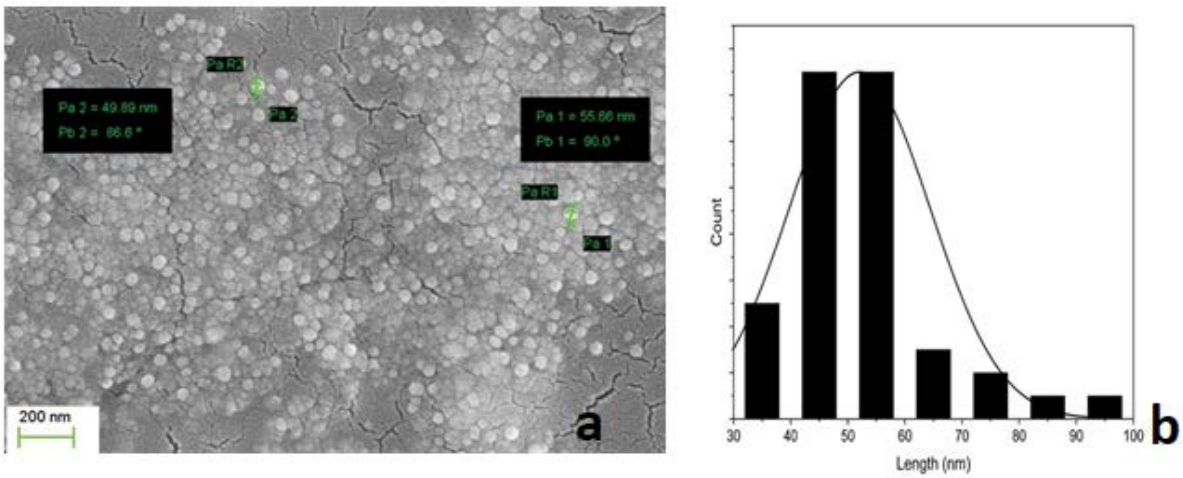


Fig. 3. FE-SEM result of AgNPs (a) FE-SEM micrograph and (b) particle-size distribution.

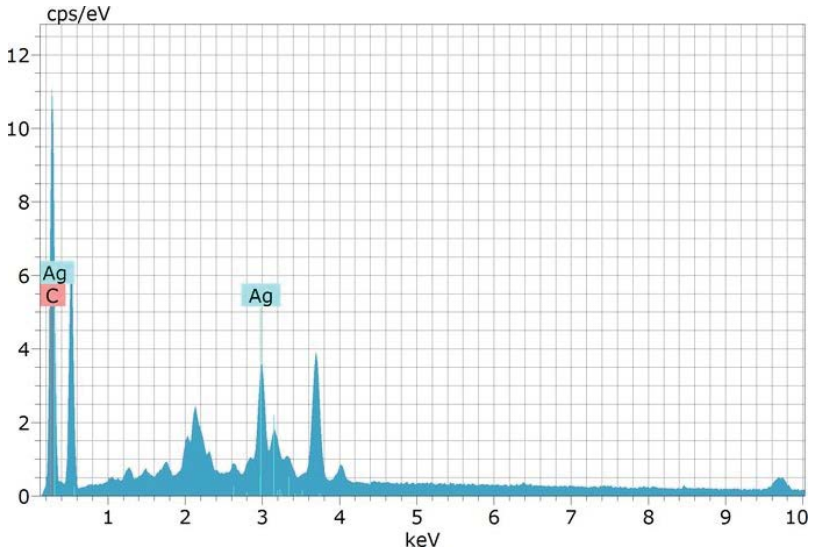


Fig. 4. Energy-dispersive X-ray spectrum.

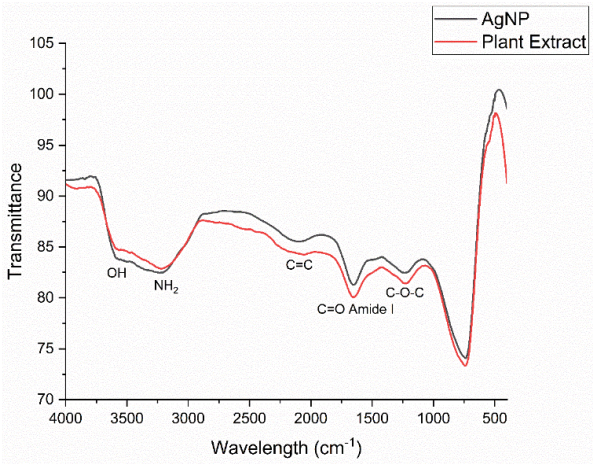


Fig. 5. Fourier-transform infrared spectrum of PPLE and AgNPs.

representing lattice plane reflections of face centered cubic lattice structure. The obtained values were compared with the JCPDS standard card no 04-0783 for silver and were found to be very close [36]. The XRD pattern confirmed the face-centred cubic structure, and the broad peak indicates the smaller crystal size of the AgNPs. The lattice constant obtained from the XRD was 4.0794 +/–0.012 Å. The lattice constant was close to the lattice constant value of the standard lattice constant of 4.086 Å [37].

### 3.2.5. pH point of zero charge of AgNPs

The pH of the silver nanoparticle plays a major role in photocatalytic reactions. The $pH_{ZPC}$ (point of zero charge pH) is the pH at which the net charge of the AgNPs becomes zero. The pH point of zero charge was determined using pH drift method by varying the pH of AgNP solutions from 2 to 12. The initial and final pH values were recorded and the difference between the same was plotted against the initial

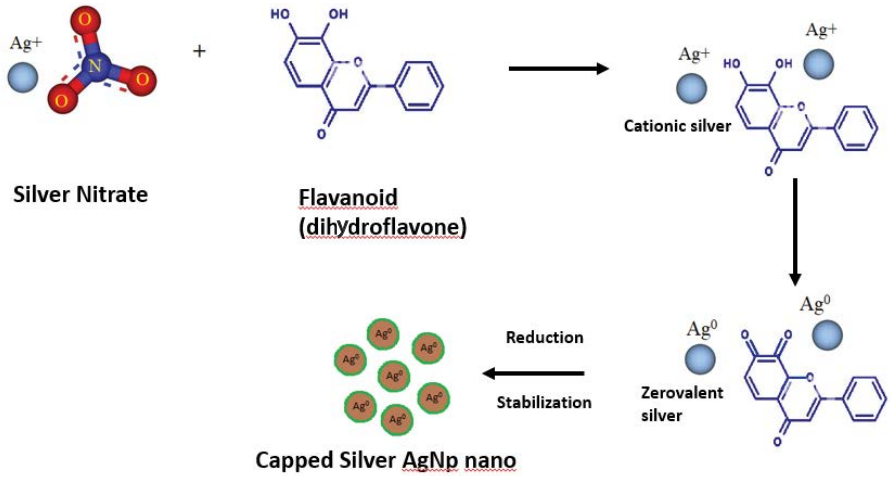


Fig. 6. Tentative mechanism of synthesis of silver nanoparticle by *Pongamia pinnata* leaf extract.

pH of the solution. The solution pH at which zero difference in pH values is observed corresponds to the point of zero charge pH.

The point of zero charge was calculated and the graph has been plotted. From Fig. 8, the $pH_{ZPC}$ of AgNPs is observed to be 8.5. It is evident that the AgNPs are predominately negatively charged. The AgNPs would obtain a net positive charge in a solution below the $pH_{ZPC}$ of pH 8.5. Acid dyes are anionic dyes a net negative charge. When AgNPs are added to the dye solution at acidic pH, the mutual attraction between the positive charge of AgNPs and the negative charge of acid dyes aids in the adsorption of the dye particles on the AgNPs thus aiding in photocatalytic degradation of the dye particles.

### 3.3. Photocatalytic studies

The photocatalytic activity of AgNPs in the dye degradation of Colomill Brilliant Red 3BN acid dye for different dye degradation parameters was studied by measuring the UV-Visible radiation absorbance of untreated and treated dye solutions. The percentage of dye degradation is tabulated in Table 1.

Fig. 9 shows the degradation of the dye before and after photocatalytic treatment. It can be observed that there is a physical colour difference in the treated dye for 2 h of 5 ppm concentration of dye solution with a catalyst concentration of 10 mg/L at 4 pH.

The effect of the initial concentration of the dye solution on photocatalytic degradation was studied with 5, 10, and 15 ppm of initial concentration. The constant parameters were catalyst concentration at 10 mg/L, pH at 7, and time of irradiation for 2 h. The UV absorption spectra of the various dye solutions before and after photocatalytic degradation are represented in Fig. 10. It is observed that 48% of 5 ppm dye was degraded at the end of the irradiation time, while 28% and 14% of dye were degraded in 10 and 15 ppm solutions, respectively. A steady decrease in the dye degradation was observed with the increase in dye concentration. For constant catalyst concentration, the active functional

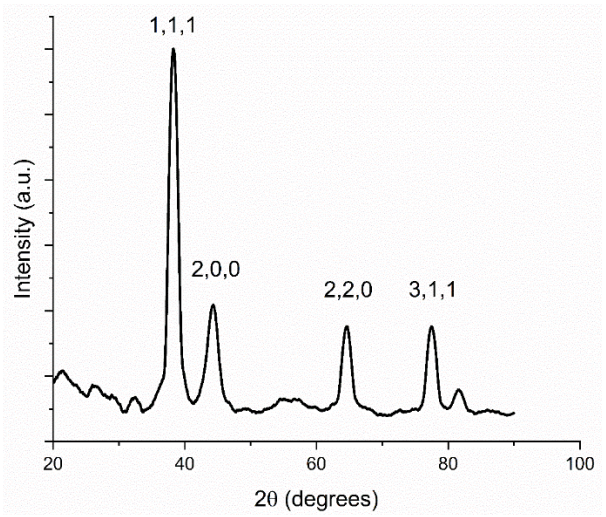


Fig. 7. X-ray diffraction pattern of AgNP.

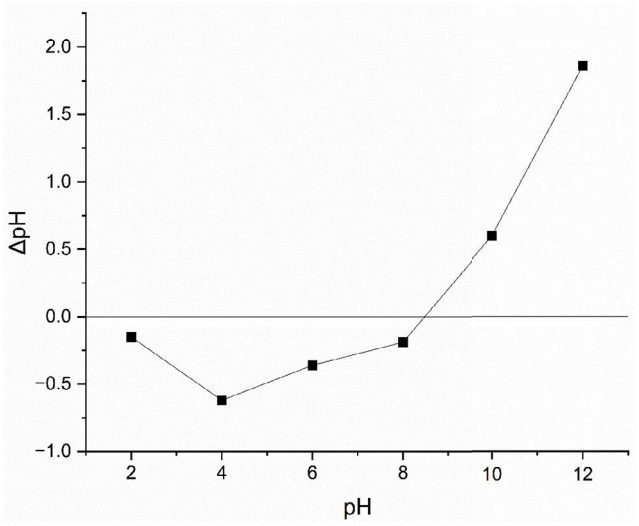


Fig. 8. pH of point of zero charge of AgNPs.

Table 1
Percentage of dye degradation for various factors affecting photocatalysis

| Dye concentration (ppm) | Catalyst concentration (mg/L) | pH | Time (h) | Dye degradation (%) |
|---|---|---|---|---|
| 5 | 10 | 7 | 2 | 48 |
| 10 | 10 | 7 | 2 | 28 |
| 15 | 10 | 7 | 2 | 14 |
| 5 | 5 | 7 | 2 | 18 |
| 5 | 10 | 7 | 2 | 48 |
| 5 | 15 | 7 | 2 | 24 |
| 5 | 10 | 4 | 2 | 74 |
| 5 | 10 | 7 | 2 | 28 |
| 5 | 10 | 10 | 2 | 12 |
| 5 | 10 | 7 | 1 | 18 |
| 5 | 10 | 7 | 2 | 48 |
| 5 | 10 | 7 | 3 | 60 |

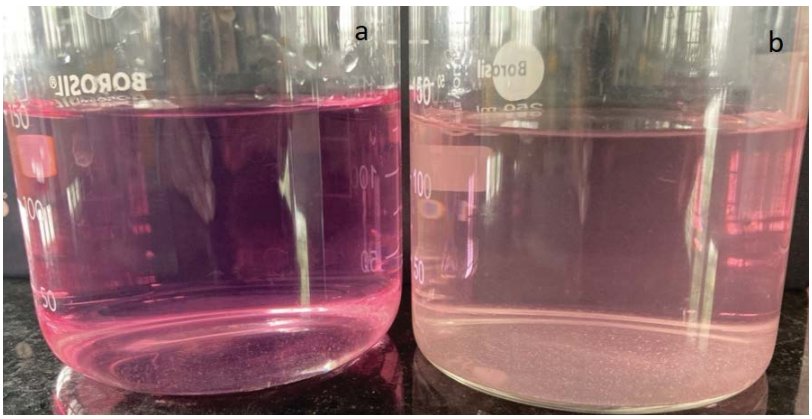


Fig. 9. Dye colour (a) before and (b) after photocatalytic treatment.

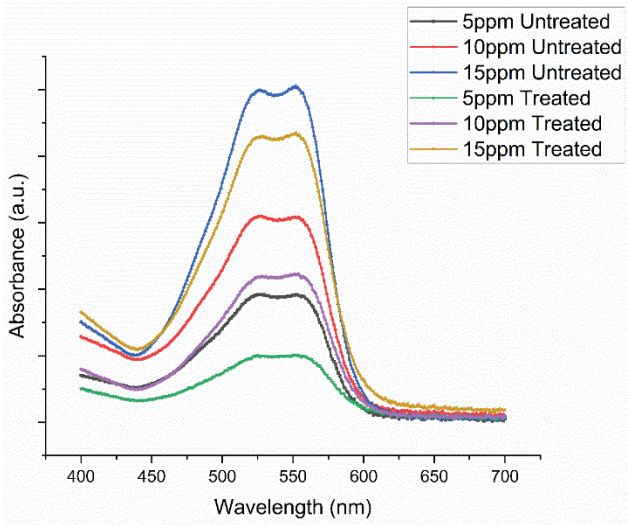


Fig. 10. Absorbance with respect to variable dye concentration of untreated and treated dye solutions.

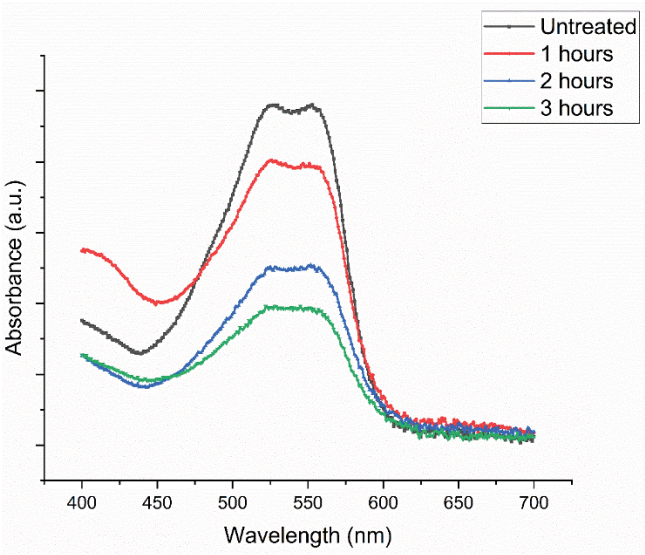


Fig. 11. Absorbance with respect to time of photocatalytic reaction.

groups present in the dye and the concentration of the dye had a direct relationship with the interaction between the photocatalyst and the dye [38]. The photocatalytic activity decreased with the increase in initial concentration, since the active sites of the photocatalyst were limited, thereby increasing the number of dye molecules competing for the active sites of the photocatalyst [39]. As the dye concentration increased, the irradiated light was predominantly absorbed by the dye instead of the photocatalyst, restricting the effective surface plasmon resonance [40].

The effect of irradiation time on the degradation of dye was studied by exposing a 5 ppm dye solution with 10 mg/L catalyst concentration at 7 pH to solar irradiation for 1, 2, and 3 h. As represented in Fig. 11, a decrease in the absorbance value was observed with an increase in irradiation time. The initial concentration of the dye solution was reduced by 18%, 48%, and 60% when the solution was irradiated for 1, 2, and 3 h, respectively. Catalytic activity increased with time. Degradation increased by 167% when irradiation time was increased from 1 h to 2 h. In contrast, the degradation increased by 25% when irradiation was increased by an hour from 2 to 3 h. The photocatalytic degradation efficiency was dependent on the size of the nanoparticle, surface structure, and the size distribution of the silver nanoparticle. There was a steady increase in the dye degradation from 1 to 2 h which was due to the redshift in the local surface plasmon resonance. During further exposure, the degradation rate was slower which was due to the surface restructuring of silver nanoparticles, and cluster formation of AgNPs which led to the blueshift of the local surface plasmon resonance [41]. Hence 2 h of irradiation is optimized for further reactions.

The concentration of the photocatalyst in the dye solution plays a major role in the reaction and degradation rate. In order to study the effect of the concentration of AgNPs as a catalyst on the degradation of 5 ppm dye at 7 pH, the concentration of AgNPs was varied as 5, 10, and 15 mg/L. The photocatalytic reactions were carried out for 2 h. As shown in Fig. 12, the initial concentration of dye was reduced by 18% when 5 mg/L AgNPs was added, while the concentration reduced by 48% and 24% when 10 and

15 mg/L were used, respectively. The degradation increased by 167% when catalyst concentration was increased from 5 to 10 mg/L but reduced by 50% when catalyst concentration was increased from 10 to 15 mg/L. The increase in the concentration of the photocatalyst resulted in the generation of a greater number of electron–hole pairs and hence faster and effective degradation of the dye was achieved [42]. At lower concentrations of the catalyst, the degradation was lesser which may be due to less accessibility of AgNPs for electron absorption in the conduction band. Similarly, it was observed that when there was an increase in photocatalytic concentration beyond 10 mg/L there was a slight decrease in degradation which may be due to the turbidity of the AgNPs clusters leading to scattering of light and blocking of light penetration inside the dye solution [43,44].

The study of pH on the effect of the photocatalytic reaction is of much importance due to the fact that pH governs the surface characteristics of the photocatalyst [45]. Acid Red 3BN dye used in this study has negatively charged sulphonic groups to enhance the solubility of the dye. Hence the electrostatic attraction between the dye and the silver nanoparticle enables the adsorption of the dye on the surface of the photocatalyst when the pH is acidic [46]. To analyze the effect of pH on the reaction, dye solutions with three different pH 4, 7, and 10 were taken for the study and it was reported that when the pH was acidic, the degradation rate of the dye was higher. The effect of pH on dye degradation was studied for a 5 ppm dye solution with 10 mg/L catalyst concentration maintained at acidic, neutral, and basic conditions. The absorbance values decreased as depicted in Fig. 13. The maximum degradation of 74% was observed at 4 pH, while degradation was 48% and 12% for solutions maintained at pH 7 and 10, respectively. The dye degradation improved with an increase in the acidity of the solution.

### 3.4. Kinetic modelling

To understand the mechanism of decolourization of dyes during photocatalytic reactions, kinetic models were used as a tool. First-order kinetics, pseudo-first-order, second-order kinetics, and pseudo-second-order kinetics were studied and rate constants for each model are tabulated in Table 2 and represented in Fig. 14a–d.

The reaction rate was directly proportional to the concentration of the reactants in first-order reaction. Among all four models listed, the first-order kinetics fitted well with the highest correlation coefficient ($R^2$) value of 0.976. The other models exhibited lower correlation coefficients than the first-order kinetics.

### 3.5. Study of changes in the morphology of AgNPs after photocatalytic treatment

There is no significant change in the morphological structure of silver nanoparticles before and after the treatment

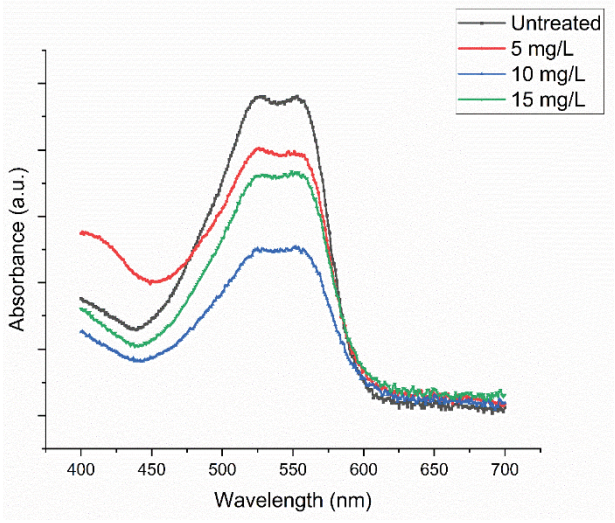


Fig. 12. Absorbance with respect to variable concentration of photocatalyst.

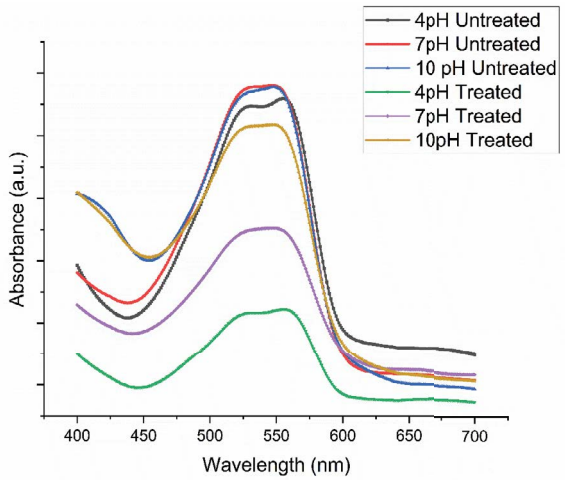


Fig. 13. Absorbance with respect to pH variation during photocatalytic degradation.

Table 2
Rate constant and $R^2$ values of various kinetic models

| Model | Formula | Rate constant | $R^2$ values |
|---|---|---|---|
| Zeroth-order reaction | $C = C_0 - kt$ | 0.00424 | 0.99244 |
| First-order | $\ln C = \ln C_0 - kt$ | 0.00577 | 0.97629 |
| Pseudo-first-order | $\ln[C_0 - C] = \ln C - kt$ | 0.0117 | 0.94818 |
| Second-order | $1/C = 1/C_0 + kt$ | 0.00807 | 0.93891 |
| Pseudo-second-order | $t/C = t/C_0 - 1/kC_0^2$ | 0.00859 | 0.9466 |

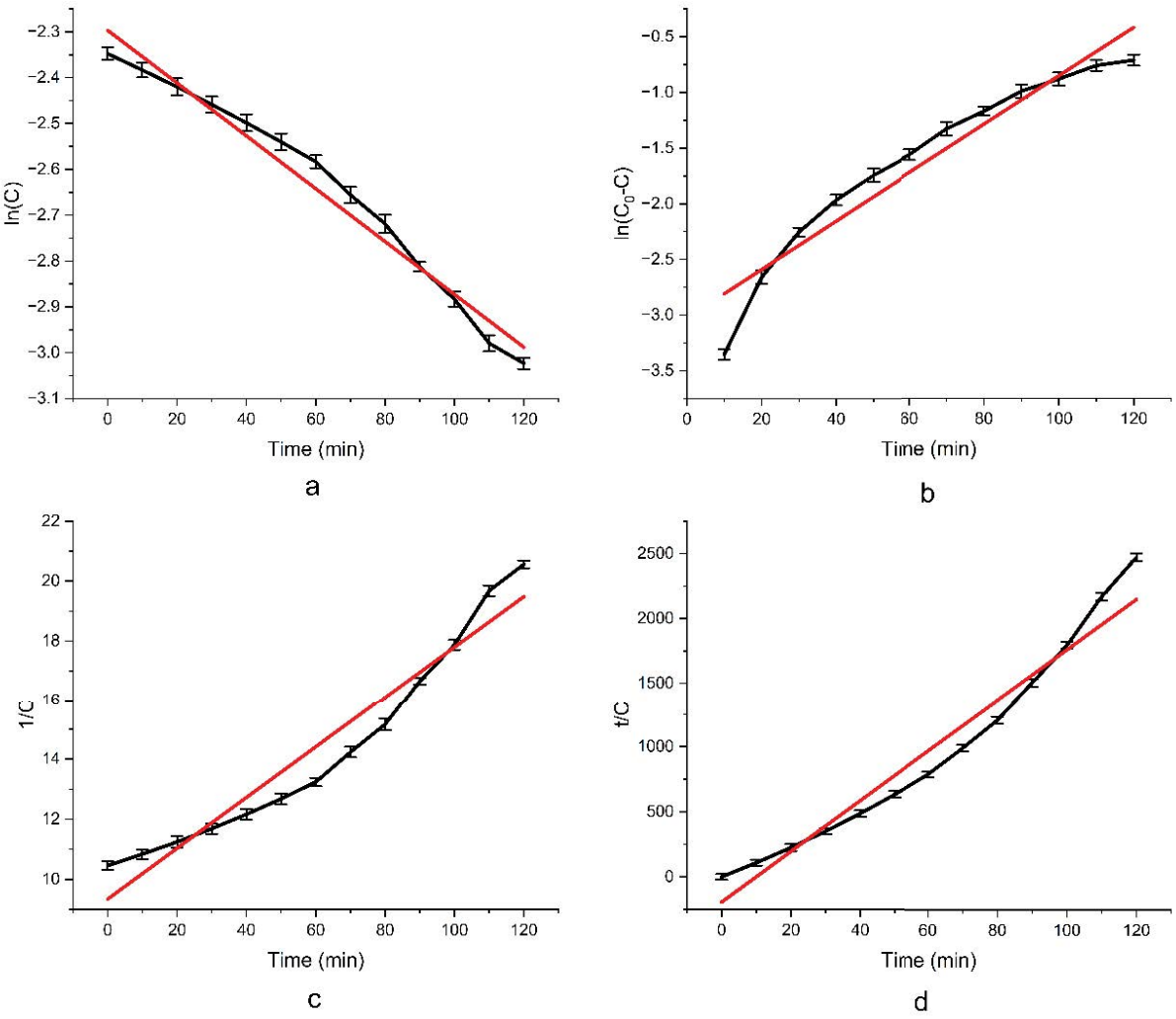


Fig. 14. Kinetic models for decolourization of C.I. Acid Red 131 (a) first-order reaction, (b) pseudo-first-order reaction, (c) second-order reaction, and (d) pseudo-second-order reaction.

as indicated in Fig. 15a and b. The particle size of AgNPs range from 20 to 80 nm with a maximum number of 50 nm particle size which is very close to the morphology of the AgNPs before photocatalytic reaction. Meanwhile the after treatment FE-SEM images reveals the dyes adhering to the silver nanoparticles. From Fig. 15c, the size of the dye can be noted as from 12 to 26 nm.

### 3.6. Stability and reusability study

In order to study the practical application of the synthesized silver nanoparticle were subjected for reusability and stability studies. The dye particles after each run was removed by centrifugation process and the obtained silver nano was reused. The reusability experiment was conducted for three successive runs. As shown in Fig. 16 even after three successive photocatalytic treatments, there is no significant difference observed in the efficiency of the photocatalyst. The morphological structure and size of the silver nanoparticles before and after the photocatalytic activity remain almost the same. From these studies, it is evident that the silver nanoparticle exhibits photostability and reusability against the dyes. This confirms the practical application of silver nanoparticles in the treatment of dye wastewater.

### 3.7. Mechanism

The possible mechanism of photocatalytic activity in the degradation of organic dyes is represented in Fig. 17.

When solar irradiation is induced in the bath containing dyes and PPLE-AgNPs, the dye gets excited and generates $e^-$ and the PPLE-AgNPs undergo non-radioactive plasmonic decay by absorbing the photons and generating excited electrons in the conduction band. This process increases the potential energy of the electrons, priming them for further reactions [47,48].

$$\text{Dye} + h\nu \rightarrow \text{Dye}^* \quad \text{(I)}$$

$$\text{AgNPs} + h\nu \rightarrow \text{AgNPs}\, e^- h^+ \quad \text{(II)}$$

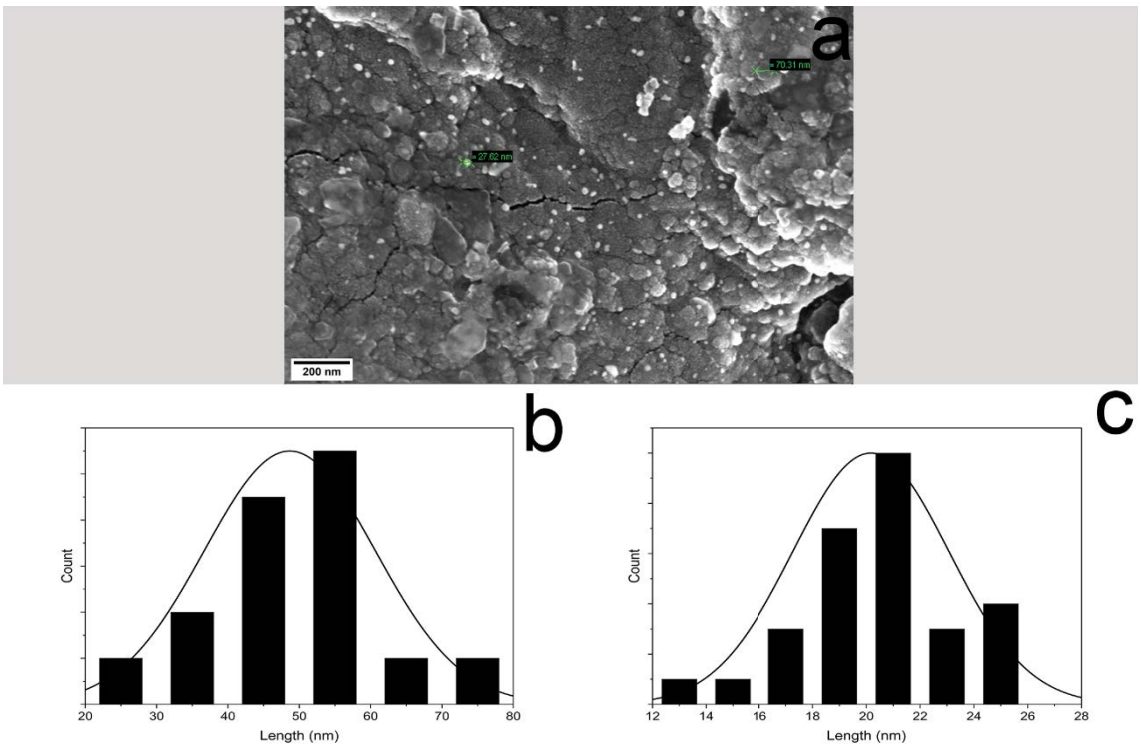


Fig. 15. FE-SEM result of AgNPs after treatment (a) FE-SEM micrograph after treatment, (b) particle-size distribution of treated AgNPs, and (c) particle-size distribution of dye particles adhering to AgNPs after treatment.

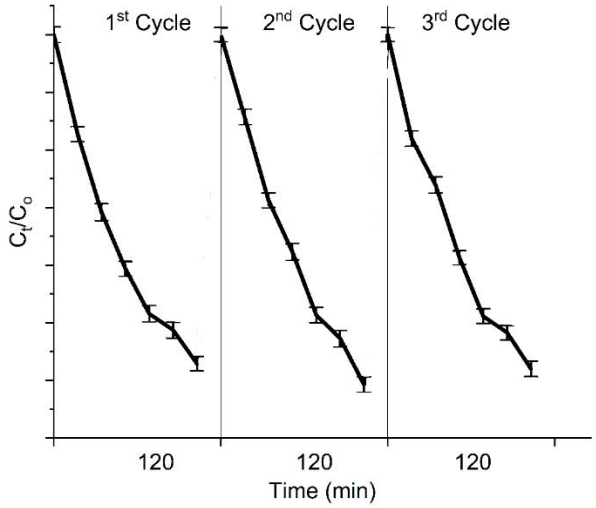


Fig. 16. Reusability study.

The acid dye molecules are adsorbed onto the surface of the silver nanoparticles, creating a localized environment where the dye molecules can interact with the nanoparticle surface and reactive species [49–51]. The excited electrons are transferred from the conduction band of the silver nanoparticles to the adsorbed dye molecules on the nanoparticle surface. This leads to the formation of electron-deficient sites on the nanoparticle surface [52].

$$\text{Dye}^* + \text{AgNPs} \rightarrow \text{Dye} + \left(\text{AgNPs}\right)e^- \quad \text{(III)}$$

The transferred electrons can react with molecular oxygen adsorbed on the silver nanoparticle surface, leading to the generation of reactive oxygen species (ROS) such as superoxide radicals ($O_2^-$) and hydroxyl radicals ($OH^\bullet$). These ROS are highly oxidative and play a crucial role in the degradation of the dye molecules [53].

$$O_2 + \left(\text{AgNPs}\right)e^- \rightarrow \text{AgNPs} + O_2^{\bullet -} \quad \text{(IV)}$$

$$O_2^{\bullet -} + H^+ \rightarrow HO_2^{\bullet} \quad \text{(V)}$$

$$2HO_2^{\bullet} \rightarrow O_2 + H_2O_2 \quad \text{(VI)}$$

$$H_2O_2 + O_2^{\bullet -} \rightarrow HO^- + HO^\bullet + O_2 \quad \text{(VII)}$$

$$\left(\text{AgNPs}\right)e^- + H_2O_2 \rightarrow HO^\bullet + HO^- \quad \text{(VIII)}$$

$$H_2O + \left(\text{AgNPs}\right)h^+ \rightarrow \text{AgNPs} + HO^\bullet + H^+ \quad \text{(IX)}$$

$$HO^- + \left(\text{AgNPs}\right)h^+ \rightarrow \text{AgNPs} + HO^\bullet \quad \text{(X)}$$

The generated ROS, particularly hydroxyl radicals ($OH^\bullet$), initiate a series of oxidative reactions with the adsorbed acid dye molecules. Hydroxyl radical abstract hydrogen atoms from the dye molecules, breaking down the chemical bonds and resulting in the degradation of the dye molecules into smaller fragments [54]. The degradation products of the acid dye are smaller and less coloured than the parent dye molecules. These degradation products are often less harmful

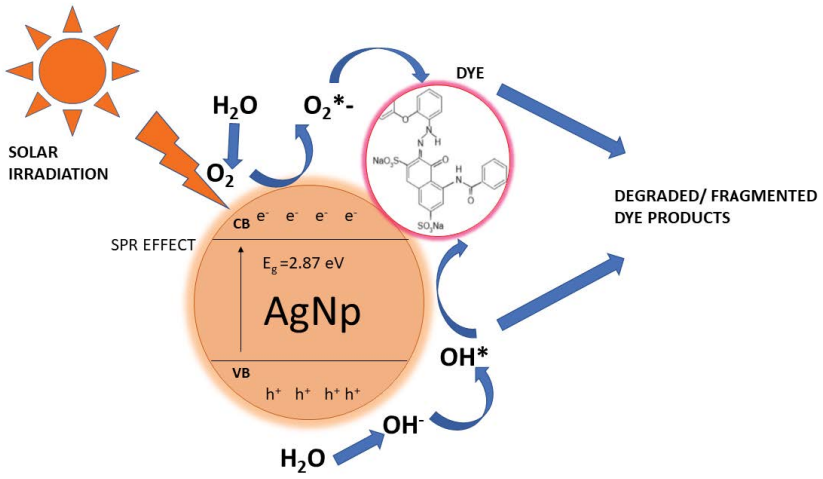


Fig. 17. Mechanism of dye degradation of Colomill Brilliant Red 3BN by photocatalytic effect of AgNP.

Table 3
Performance comparison of various nanoparticles for degradation of various dyes

| Catalyst | Dye | Concentration of dye | Catalyst loading | Catalytic efficiency (%) | Reaction time (min) | Rate constant ($min^{-1}$) | References |
|---|---|---|---|---|---|---|---|
| $Ag/Ag_2O$ NP | Methylene blue | 1.0 mg/L | 10 mg/L | 93 | 360 | 0.0015 | [56] |
| AgNP | Methylene blue | | | 94.50 | 60 | – | [57] |
| | Rhodamine B | 1.0 mg/L | 0.001 mg | 96.30 | 35 | – | |
| AgNP | Methylene blue | 60 ppm | 1.8 mL | 82.80 | 180 | 0.011 | [58] |
| His-AgNP | Methylene blue | 20 ppm | 5 mg/L | 98 | 40 | 0.3508 | [28] |
| | Methyl orange | 20 ppm | 5 mg/L | 97 | 100 | 0.3977 | |
| AgNPs | Methylene blue | 10 mg/L | 0.1 mg/L | – | 1,440 | 0.00144 | [36] |
| | Methyl orange | 10 mg/L | 0.1 mg/L | – | 1,440 | 0.00186 | |
| | | 10 mg/L | 0.1 mg/L | – | 1,440 | 0.00103 | |
| AgNPs | Direct blue | 100 mg/L | 100 mg/100 mL | 39.96 | 60 | – | [59] |
| | Methyl red | 100 mg/L | | 69.87 | 60 | – | |
| | Reactive blue 5 | 100 mg/L | | 50.31 | 60 | – | |
| AgNPs/Peroxodi-sulphide | Methyl orange | $5 \times 10^{-5}$ mol/$dm^3$ | $1 \times 10^{-8}$ mol/$dm^3$ | | 45 | – | [60] |
| AgNPs | Reactive blue 19 | 30 ppm | 10 mg | 88.5 | 180 | $1.23 \times 10^{-2}$ | [17] |
| | Reactive yellow 186 | 30 ppm | 10 mg | 86.6 | 180 | $1.03 \times 10^{-2}$ | |
| AgNPs/$NaBH_4$ | Methyl orange | 75 mg/L | 0.01 mL | 90 | 10 | 0.247 | [61] |
| | Methylene blue | 75 mg/L | 0.01 mL | 90 | 20 | 0.105 | |
| | Congo red | 75 mg/L | 0.01 mL | 90 | 20 | 0.101 | |
| AgNPs | Eosin Y | 1 mM | 1 mg/L | 93.8 | 180 | – | [62] |
| AgNPs/$NaB_H4$ | C.I. Acid Red 249 | $6.6–21.4 \times 10^{-5}$ M | 1.12 mL | 96.20 | 26 | – | [63] |
| AgNP doped $TiO_2$ | Acid Red 88 | $5 \times 10^{-5}$ M@pH 4.8 | 0.6 g/L | 90.54 | 60 | – | [64] |
| AgNPs | Eosin Y | 10 mg/L | 50 mg | 97 | 60 | – | [65] |
| AgNPs | C.I. Acid Red | 5 ppm | 10 mg/L | 74 | 120 | 0.00577 | Present study |

to the environment. The byproducts can further undergo secondary reactions or mineralization into harmless substances [55].

The energy band gap of the synthesized silver nanoparticle was obtained using Eq. (3):

$$\text{Energy band gap}\left(E_g\right) = \frac{hc}{\lambda_{\max}} \tag{3}$$

where $h$ = Planck's constant, $c$ = speed of light, $\lambda_{max}$ = maximum wavelength of light.

Hence the maximum wavelength obtained for PPLE-AgNP is 432 nm and the energy band gap is 2.87 eV. The valance band and conduction band potential were calculated using Mulliken electronegativity and band gap of the synthesized nanoparticle was found to be 1.3408 and –1.5291 eV, respectively. The photocatalytic studies of the PPLE-AgNPs shows that the degradation of dyes is due to the reactive oxygen species generated by surface plasmon resonance and creation of positive holes in the silver nanoparticle.

### *3.8. Comparative study*

Finally, the test results were compared with the previous findings to find out the effectiveness of the AgNPs as photocatalysts. In most of the cases, cationic dyes were used for the photocatalytic study. From the comparison data Table 3, it is noted that the easily degradable cationic dyes like methyl orange (molecular weight - 327.33 g/mol), methylene blue (molecular weight - 319.85 g/mol), Rhodamine B (molecular weight - 479.02 g/mol), were used for the degradable studies. This may be because the diffusion rates of their dyes are higher than those of the textile dyes, due to their low molecular weight [17]. The Colomill Brilliant Red 3BN, (molecular weight - 677.6 g/mol) which is widely used by the industry was taken for the study and the dye removal efficiency is comparable with the other studies. In this study, no other reducing agents were used, hence the process is purely based on the photocatalytic activity of AgNP alone.

## 4. Conclusion

In this present study, *P. pinnata* leaf extract PPLE was successfully used as a reducing and capping agent for the synthesis of AgNPs from $AgNO_3$ under simple, easy, and rapid environmentally friendly methods. The UV-Vis results confirm the formation of AgNPs at a peak value of 432 nm. From FE-SEM analysis, the structure of the AgNPs was found to be spherical and the maximum particle size range is 50 nm. The elemental study confirms the presence of AgNP at 3.0 eV. The photocatalytic studies were efficient at 5 ppm dye concentration, 10 mg/L of catalyst concentration at a pH of around 4, and a time is 120 min. The efficiency was found to be 74% which is comparable to higher molecular-weight compound dyes. The kinetic reactions followed pseudo-first-order with the rate constant of 0.00577 $min^{-1}$. This method has several advantages the usage of green synthesis, without using and reducing agents or chemicals, eliminating the need for organic solvents, and readily can be integrated for the purification of textile wastewater treatment which is cost-effective and the photocatalyst can be reused.

## References

[1] L. Lin, H. Yang, X. Xu, Effects of water pollution on human health and disease heterogeneity: a review, Front. Environ. Sci., 10 (2022) 880246, doi: 10.3389/fenvs.2022.880246.
[2] X. Xu, H. Yang, C. Li, Theoretical model and actual characteristics of air pollution affecting health cost: a review, Int. J. Environ. Res. Public Health, 19 (2022) 3532, doi: 10.3390/ijerph19063532.
[3] S. Khan, A. Malik, Toxicity evaluation of textile effluents and role of native soil bacterium in biodegradation of a textile dye, Environ. Sci. Pollut. Res., 25 (2018) 4446–4458.
[4] K. Shirvanimoghaddam, B. Motamed, S. Ramakrishna, M. Naebe, Death by waste: fashion and textile circular economy case, Sci. Total Environ., 718 (2020) 137317, doi: 10.1016/j.scitotenv.2020.137317.
[5] S. Popli, U. Patel, Destruction of azo dyes by anaerobic and aerobic sequential biological treatment: a review, Int. J. Environ. Sci. Technol., 12 (2014) 405–420.
[6] K. Siddique, M. Rizwan, M.J. Shahid, S. Ali, R. Ahmad, H. Rizvi, Textile Wastewater Treatment Options: A Critical Review, N. Anjum, S. Gill, N. Tuteja, Eds., Enhancing Cleanup of Environmental Pollutants, Springer, Cham, 2017, pp. 183–207.
[7] T. Robinson, G. McMullan, R. Marchant, P. Nigam, Remediation of dyes in textile effluent: a critical review on current treatment technologies with a proposed alternative, Bioresour. Technol., 77 (2001) 247–255.
[8] S. Mukherji, J. Ruparelia, S. Agnihotri, Antimicrobial Activity of Silver and Copper Nanoparticles: Variation in Sensitivity Across Various Strains of Bacteria and Fungi, N. Cioffi, M. Rai, Eds., Nano-antimicrobials: progress and prospects, Springer-Verlag, Berlin, Heidelberg, 2012, pp. 225–251.
[9] X. Li, X. Jin, N. Zhao, I. Angelidaki, Y. Zhang, Novel bio-electro-Fenton technology for azo dye wastewater treatment using microbial reverse-electrodialysis electrolysis cell, Bioresour. Technol., 228 (2017) 322–329.
[10] S. Agnihotri, N.K. Dhiman, A. Tripathi, Antimicrobial Surface Modification of Polymeric Biomaterials, A. Tiwari, Ed., Handbook of Antimicrobial Coatings, Elsevier, New York, 2018, pp. 435–486.
[11] M.S. Akhtar, J. Panwar, Y.S. Yun, Biogenic synthesis of metallic nanoparticles by plant extracts, ACS Sustainable Chem. Eng., 1 (2013) 591–602.
[12] R.G. Saratale, I. Karuppusamy, G.S. Saratale, A. Pugazhendhi, G. Kumar, Y. Park, G.S. Ghodake, R.N. Bhargava, J.R. Banu, H.S. Shin, A comprehensive review on green nanomaterials using biological systems: recent perception and their future applications, Colloids Surf., B, 170 (2018) 20–35.
[13] P. Mukherjee, A. Ahmad, D. Mandal, S. Senapati, S.R. Sainkar, M.I. Khan, R. Parishcha, R. Ajaykumar, M. Alam, R. Kumar, Fungus mediated synthesis of silver nanoparticles and their immobilization in the mycelial matrix: a novel biological approach to nanoparticle synthesis, Nano Lett., 1 (2001) 515–519.
[14] S. Ahmed, M. Ahmad, B.L. Swami, S. Ikram, A review on plants extract mediated synthesis of silver nanoparticles for antimicrobial applications: a green expertise, J. Adv. Res., 17 (2016) 17–28.
[15] J. Singh, N. Singh, A. Rathi, D. Kukkar, M. Rawat, Facile approach to synthesize and characterization of silver nanoparticles by using mulberry leaves extract in aqueous medium and its application in antimicrobial activity, J. Nanostruct., 7 (2017) 134–140.
[16] C. Ramteke, T. Chakrabarti, B.K. Sarangi, R. Pandey, Synthesis of silver nanoparticles from the aqueous extract of leaves of *Ocimum sanctum* for enhanced antibacterial activity, J. Chem., 2013 (2013) 278925, doi: 10.1155/2013/278925.
[17] J. Singh, P. Kukkar, H. Sammi, M. Rawat, G. Singh, D. Kukkar, Enhanced catalytic reduction of 4-nitrophenol and Congo red dye by silver nanoparticles prepared from *Azadirachta indica* leaf extract under direct sunlight exposure, Part. Sci. Technol., 37 (2019) 434–443.
[18] J. Singh, G. Kaur, P. Kaur, R. Bajaj, M. Rawat, A review on green synthesis and characterization of silver nanoparticles and their applications: a green nanoworld, World J. Pharm. Pharm. Sci., 7 (2016) 730–762.
[19] N.A.N. Mohamad, N.A. Arham, J. Jai, A. Hadi, Plant extract as reducing agent in synthesis of metallic nanoparticles: a review, Adv. Mater. Res., 832 (2013) 350–355.
[20] F. Mujeeb, P. Bajpai, N. Pathak, Phytochemical evaluation, antimicrobial activity, and determination of bioactive components from leaves of *Aegle marmelos*, Biomed. Res. Int., 2014 (2014) 497606, doi: 10.1155/2014/497606.
[21] S. Kothari, V. Mishra, S. Bharat, S.D. Tonpay, Antimicrobial activity and phytochemical screening of serial extracts from

leaves of *Aegle marmelos* (Linn.), Acta Pol. Pharm.–Drug Res., 68 (2011) 687–692.
[22] V.K. Bajpai, P. Agrawal, B.H. Bang, Y.H. Park, Phytochemical analysis, antioxidant and antilipid peroxidation effects of a medicinal plant, *Adhatoda vasica*, Front. Life Sci., 8 (2015) 305–312.
[23] S. Sankhalkar, V. Vernekar, Quantitative and qualitative analysis of phenolic and flavonoid content in *Moringa oleifera* Lam and *Ocimum tenuiflorum* L., Pharmacogn. Res., 8 (2016) 16–21.
[24] S. Agnihotri, S. Mukherji, S. Mukherji, Size-controlled silver nanoparticles synthesized over the range 5–100 nm using the same protocol and their antibacterial efficacy, RSC Adv., 4 (2014) 3974–3983.
[25] S. Bharti, S. Agnihotri, S. Mukherji, S. Mukherji, Effectiveness of immobilized silver nanoparticles in inactivation of pathogenic bacteria, J. Environ. Res. Dev., 9 (2015) 849–856.
[26] M. Beg, A. Maji, A.K. Mandal, S. Das, M.N. Aktara, P.K. Jha, M. Hossain, Green synthesis of silver nanoparticles using *Pongamia pinnata* seed: characterization, antibacterial property, and spectroscopic investigation of interaction with human serum albumin, J. Mol. Recognit., 30 (2017) e2565, doi: 10.1002/jmr.2565.
[27] K. Kalimuthu, R.S. Babu, D. Venkataraman, M. Bilal, S. Gurunathan, Biosynthesis of silver nanocrystals by *Bacillus licheniformis*, Colloids Surf., B, 65 (2008) 150–153.
[28] D. Khwannimit, R. Maungchang, P. Rattanakit, Green synthesis of silver nanoparticles using *Clitoria ternatea* flower: an efficient catalyst for removal of Methyl orange, Int. J. Environ. Anal. Chem., 102 (2020) 5247–5263.
[29] W. Routray, V. Orsat, Blueberries and their anthocyanins: factors affecting biosynthesis and properties, Compr. Rev. Food Sci. Food Saf., 10 (2011) 303–320.
[30] M.G. Guzmán, J. Dille, S. Godet, Synthesis of silver nanoparticles by chemical reduction method and their antibacterial activity, Int. J. Chem. Biomol. Eng., 2 (2009) 104–111.
[31] S.R. Arote, P.G. Yeole, *Pongamia pinnata* L: a comprehensive review, Int. J. Pharm. Tech. Res., 2 (2010) 2283–2290.
[32] R.S. Priya, D. Geetha, P.S. Ramesh, Antioxidant activity of chemically synthesized AgNPs and biosynthesized *Pongamia pinnata* leaf extract mediated AgNPs – a comparative study, Ecotoxicol. Environ. Saf., 134 (2016) 308–318.
[33] R.W. Raut, N.S. Kolekar, J.R. Lakkakula, V.D. Mendhulkar, S.B. Kashid, Extracellular synthesis of silver nanoparticles using dried leaves of *Pongamia pinnata* (L) pierre, Nano-Micro Lett., 2 (2010) 106–113.
[34] P. Trouillas, P. Marsal, D. Siri, R. Lazzaroni, J.L. Duroux, A DFT study of the reactivity of OH groups in quercetin and taxifolin antioxidants: the specificity of the 3-OH site, Food Chem., 97 (2006) 679–688.
[35] M. Sharma, S. Yadav, N. Ganesh, M.M. Srivastava, S. Srivastava, Biofabrication and characterization of flavonoid-loaded Ag, Au, Au–Ag bimetallic nanoparticles using seed extract of the plant *Madhuca longifolia* for the enhancement in wound healing bio-efficacy, Prog. Biomater., 8 (2019) 51–63.
[36] K. Jyoti, M. Baunthiyal, A. Singh, Characterization of silver nanoparticles synthesized using *Urtica dioica* Linn. leaves and their synergistic effects with antibiotics, J. Radiat. Res. Appl. Sci., 9 (2016) 217–227.
[37] U. Farooq, J. Ahmed, S.M. Alshehri, T. Ahmad, High surface area sodium tantalate nanoparticles with enhanced photocatalytic and electrical properties prepared through polymeric citrate precursor route, ACS Omega, 4 (2019) 19408–19419.
[38] H. Anwer, A. Mahmood, J. Lee, K.H. Kim, J.W. Park, A.C. Yip, Photocatalysts for degradation of dyes in industrial effluents: opportunities and challenges, Nano Res., 12 (2019) 955–972.
[39] A.Y. Zhang, W.K. Wang, D.N. Pei, H.Q. Yu, Degradation of refractory pollutants under solar light irradiation by a robust and self-protected ZnO/CdS/$TiO_2$ hybrid photocatalyst, Water Res., 92 (2016) 78–86.
[40] X.R. Li, J.G. Wang, Y. Men, Z.F. Bian, $TiO_2$ mesocrystal with exposed (001) facets and CdS quantum dots as an active visible photocatalyst for selective oxidation reactions, Appl. Catal., B, 187 (2016) 115–121.
[41] G. Kumari, R. Kamarudheen, E. Zoethout, A. Baldi, Photocatalytic surface restructuring in individual silver nanoparticles, ACS Catal., 11 (2011) 3478–3486.
[42] J.J. Jung, J.W. Jang, J.W. Park, Effect of generation growth on photocatalytic activity of nano $TiO_2$-magnetic cored dendrimers, J. Ind. Eng. Chem., 44 (2016) 52–59.
[43] H. Answer, J.W. Park, Synthesis and characterization of a heterojunction rGO/$ZrO_2$/$Ag_3PO_4$ nanocomposite for degradation of organic contaminants, J. Hazard. Mater., 358 (2018) 416–426.
[44] F.A. Alharthi, A.A. Alghamdi, N. Al-Zaqri, H.S. Alanazi, A.A. Alsyahi, A.E. Marghany, N. Ahmad, Facile one-pot green synthesis of Ag–ZnO nanocomposites using potato peel and their Ag concentration dependent photocatalytic properties, Sci. Rep., 10 (2020) 20229, doi: 10.1038/s41598-020-77426-y.
[45] F. Azeez, E. Al-Hetlani, M. Arafa, Y. Abdelmonem, A.A. Nazeer, M.O. Amin, M. Madkour, The effect of surface charge on photocatalytic degradation of methylene blue dye using chargeable titania nanoparticles, Sci. Rep., 8 (2018) 7104, doi: 10.1038/s41598-018-25673-5.
[46] M. Siddique, R. Khan, A.F. Khan, R. Farooq, Improved photocatalytic activity of $TiO_2$ coupling ultrasound for Reactive Blue 19 degradation, J. Chem. Soc. Pak., 36 (2014) 37–43.
[47] T. Theivasanthi, M. Alagar, Electrolytic synthesis and characterization of silver nanopowder, Nano Biomed. Eng., 4 (2012) 58–65.
[48] T. Ahmad, R. Phul, P. Alam, I.H. Lone, M. Shahazad, J. Ahmed, T. Ahamad, S.M. Alshehri, Dielectric, optical and enhanced photocatalytic properties of $CuCrO_2$ nanoparticles, RSC Adv., 7 (2017) 27549–27557.
[49] S. Marimuthu, A.J. Antonisamy, S. Malayandi, K. Rajendran, P.C. Tsai, A. Pugazhendhi, V.K. Ponnusamy, Silver nanoparticles in dye effluent treatment: a review on synthesis, treatment methods, mechanisms, photocatalytic degradation, toxic effects and mitigation of toxicity, J. Photochem. Photobiol., B, 205 (2020) 111823, doi: 10.1016/j.jphotobiol.2020.111823.
[50] M.S. Sumi, A. Devadiga, V. Shetty, M.B. Saidutta, Solar photocatalytically active, engineered silver nanoparticle synthesis using aqueous extract of mesocarp of *Cocos nucifera* (Red Spicata Dwarf), J. Exp. Nanosci., 12 (2016) 1–19.
[51] M. Mavaei, A. Chahardoli, Y. Shokoohinia, A. Khoshroo, A. Fattahi, One-step synthesized silver nanoparticles using isoimperatorin: evaluation of photocatalytic, and electrochemical activities, Sci. Rep., 10 (2020) 1762, doi: 10.1038/s41598-020-58697-x.
[52] A. Manuel, A. Kirkey, N. Mahdi, K. Shankar, Plexcitonics – fundamental principles and optoelectronic applications, J. Mater. Chem. C, 7 (2018) 1821–1853.
[53] A. Liang, L. Qingye, W. Guiqing, J. Zhiliang, The surface-plasmon-resonance effect of nanogold/silver and its analytical applications, TrAC, Trends Anal. Chem., 37 (2012) 32–47.
[54] S. Li, X. Bing, C. Jialin, L. Yanping, Z. Junlei, W. Hengwei, L. Jianshe, Constructing a plasmonic p-n heterojunction photocatalyst of 3D Ag/$Ag_6Si_2O_7$/$Bi_2MoO_6$ for efficiently removing broad-spectrum antibiotics, Sep. Purif. Technol., 254 (2021) 117579, doi: 10.1016/j.seppur.2020.117579.
[55] V.G. Belessiotis, G.K. Ahanassios, Plasmonic silver (Ag)-based photocatalysts for $H_2$ production and $CO_2$ conversion: review, analysis and perspectives, Renewable Energy, 195 (2022) 497–515.
[56] N.K. Nasab, Z. Sabouri, S. Ghazal, M. Darroudi, Green-based synthesis of mixed-phase silver nanoparticles as an effective photocatalyst and investigation of their antibacterial properties, J. Mol. Struct., 1203 (2020) 127411, doi: 10.1016/j.molstruc.2019.127411.
[57] F. Naaz, U. Farooq, M.M. Khan, T. Ahmad, Multifunctional efficacy of environmentally benign silver nanospheres for organic transformation, photocatalysis, and water remediation, ACS Omega, 5 (2020) 26063–26076.
[58] J. Singh, A.S. Dhaliwal, Plasmon-induced photocatalytic degradation of methylene blue dye using biosynthesized silver nanoparticles as photocatalyst, Environ. Technol., 41 (2018) 1520–1534.

[59] T. Ahmed, M. Noman, M. Shahid, M.B.K. Niazi, S. Hussain, N. Manzoor, B. Li, Green synthesis of silver nanoparticles transformed synthetic textile dye into less toxic intermediate molecules through LC-MS analysis and treated the actual wastewater, Environ. Res., 191 (2020) 110142, doi: 10.1016/j.envres.2020.110142.
[60] N. Nagar, V. Devra, A kinetic study on the degradation and biodegradability of silver nanoparticles catalyzed Methyl orange and textile effluents, Heliyon, 5 (2019) e01356, doi: 10.1016/j.heliyon.2019.e01356.
[61] M. Sarkar, S. Denrah, M. Das, M. Das, Statistical optimization of bio-mediated silver nanoparticles synthesis for use in catalytic degradation of some azo dyes, Chem. Phys. Impact, 3 (2021) 100053, doi: 10.1016/j.chphi.2021.100053.
[62] S. Raina, A. Roy, N. Bharadvaja, Degradation of dyes using biologically synthesized silver and copper nanoparticles, Environ. Nanotechnol. Monit. Manage., 13 (2020) 100278, doi: 10.1016/j.enmm.2019.100278.
[63] A. Nautiyal, S.R. Shukla, Silver nanoparticles catalyzed reductive decolorization of spent dye bath containing acid dye and its reuse in dyeing, J. Water Process Eng., 22 (2018) 276–285.
[64] S. Anandan, P.S. Kumar, N. Pugazhenthiran, J. Madhavan, P. Maruthamuthu, Effect of loaded silver nanoparticles on $TiO_2$ for photocatalytic degradation of Acid Red 88, Sol. Energy Mater. Sol. Cells, 92 (2008) 929–937.
[65] R. Karthik, M. Govindasamy, S.M. Chen, Y.H. Cheng, P. Muthukrishnan, S. Padmavathy, A. Elangovan, Biosynthesis of silver nanoparticles by using *Camellia japonica* leaf extract for the electrocatalytic reduction of nitrobenzene and photocatalytic degradation of Eosin-Y, J. Photochem. Photobiol., B, 170 (2017) 164–172.